Dynamical characterization of chaotic itinerancy in a three-mode laser subjected to frequency-shifted optical feedback

Yoshihiko Miyasaka,* Kenju Otsuka, and Tsuyoshi Maniwa
Department of Human and Information Science, Tokai University, 1117 Kitakaname, Hiratsuka, Kanagawa 259-1292, Japan

Jing-Yuan Ko
Department of Physics, National Kaohsiung Normal University, Kaohsiung, Taiwan
(Received 22 April 2004; published 22 October 2004)

We investigated chaotic dynamics in a microchip three-mode solid-state laser subjected to frequency-shifted optical feedback. When the frequency shift was tuned to harmonic frequencies of the relaxation oscillation, a bifurcation from a periodic sustained relaxation oscillation ("soft-mode") state to a chaotic spiking ("hard-mode") state via a chaotic itinerancy was observed as the feedback intensity was increased. Dynamic characterizations of modal interplay and self-induced switching between the soft- and hard-mode chaotic states over times (i.e., chaotic itinerancy) were carried out by the information circulation analysis and joint time-frequency analysis of long-term experimental time series. Drastic changes in information transfer rates among oscillating modes and occasional frequency locking among periodicities of two chaotic states associated with switchings were identified in chaotic itinerancy. Essential dynamical behaviors were reproduced by numerical simulation.

DOI: 10.1103/PhysRevE.70.046208 PACS number(s): 05.45.−a, 42.55.Xi, 42.60.Mi, 42.65.Sf

I. INTRODUCTION

During the past decade, chaotic itinerancy has been recognized to be universal dynamics in a wide range of disciplines of high-dimensional dynamical systems, such as Hamiltonian systems, physicochemical experiments, biology and brain, and showing self-induced switching motion among the ruins of coexisting dynamic states through high-dimensional chaos [1]. Chaotic itinerancy (CI) was numerically discovered in laser systems at first [2,3], and then it was independently proposed in a coupled map lattice [4,5] and in neural networks [6]. The first experimental evidence of CI was reported in a nonlinear optical resonator containing a photorefractive cell by Arecchi *et al.* [7] and he initiated the concept of "dry hydrodynamics" in optics [8] including CI, the transverse effect, and other nonlinear optical dynamics. CI was also demonstrated experimentally in such laser systems as a laser diode subjected to optical feedback (Lang-Kobayashi system) [9], a self-pulsating multimode laser with intracavity second-harmonic generation [10], and a single-mode laser subjected to frequency-shifted optical feedback [11]. On the other hand, much effort has gone into characterizing complex behaviors like chaotic itinerancy in high-dimensional nonlinear systems. Two promising methods based on information theory have been proposed for high-dimensional systems by introducing cross-information flow rates [12], "coarse-grained" dynamic information transfer rates [13], and information circulations among many coupled elements [14].

In this paper, we study chaotic itinerancy among soft- and hard-mode chaotic states in a laser-diode-pumped three-mode microchip solid-state laser subjected to frequency-shifted optical feedback [11], focusing on the dynamic interplay among oscillating modes. Dynamic characterizations in terms of information circulation and joint time-frequency analyses of experimental time series were carried out to identify information flows among modes and a switching scenario between two dynamic states over times. The paper is organized as follows: The experimental setup and measurement procedures are presented in Sec. II. Experimental results such as an example bifurcation diagram, typical pulsation wave forms, Poincaré sections, information circulation, and joint time-frequency analyses of experimental time series are demonstrated in Sec. III. In Sec. IV, model equations of multimode lasers subjected to frequency-shifted optical feedback are derived and numerical results, which reproduce the observed phenomena qualitatively, are presented. Section V summaries the results and discusses the physical significance of the observed nonlinear dynamics.

II. EXPERIMENTAL SCHEME

In the work described here, we used a free-running stoichiometric $LiNdP_4O_{12}$ (LNP) laser, operating on the ${}^4F_{3/2}(1) \rightarrow {}^4I_{11/2}(1,2,3)$ transitions around the 1100-nm wavelength. In this system, multilongitudinal modes can oscillate on the different transitions forming multiple-Λ schemes, because the reabsorption effect is enhanced due to higher Nd densities in the lower manifolds, ${}^4I_{11/2}$, inherent in LNP lasers [15]. We demonstrated self-induced pulsations featuring locking of modal pulsation frequencies, multidimensional quasiperiodic pulsations, and the formation of an intermode information network, in high-pump-power regimes where quantum interference effects among lower-level atoms are significant [15].

It is well known that free-running multimode solid-state lasers with spatial hole burning of population inversions exhibit an inherent antiphase dynamics in which each mode features N relaxation oscillation components (N, number of

*Electronic address: ootsuka@keyaki.cc.tokai-u.ac.jp

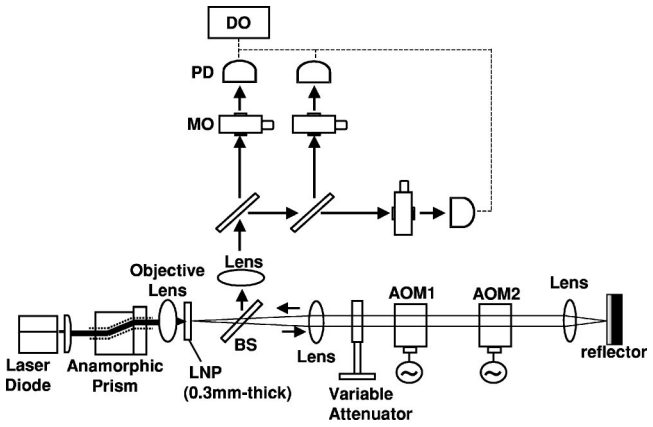

FIG. 1. Experimental setup of a microchip multimode LNP laser subjected to frequency-shifted optical feedback. LNP, $LiNdP_4O_{12}$ laser; BS, beam splitter; AOM, acoustooptic modulator; MO, monochrometer; PD, photodiode; DO, digital oscilloscope.

oscillating modes) $f_{RO} > f_2 > \cdots > f_N$ while lower-frequency components except for the highest McCumber frequency f_{RO}, appearing through cross-saturation dynamics are strongly suppressed for the total output [16]. When pump or loss modulation is applied to such lasers, chaotic oscillations are easily obtained by tuning the modulation frequency to f_{RO} [16]. On the other hand, we found that chaotic itinerancy can take place when the modulation frequency was tuned to the harmonic frequencies of relaxation oscillations—i.e., $f_s = nf_{RO}$—in a single-mode laser by means of frequency-shifted optical feedback [11], in which the laser is equivalently loss modulated at f_s.

In the present work, on the other hand, the multimode LNP laser was operated below the Hopf bifurcation threshold and chaotic behaviors were induced by frequency-shifted optical feedback. In this scheme, the chaotic itinerancy between chaotic relaxation oscillations ("soft" mode) born from a lasing stationary state and spiking oscillations ("hard" mode) built up from a nonlasing stationary state is expected to occur similar to the single-mode regime [11]. If this is the case, the system could provide a promising model for investigating multimode chaotic itinerancy among these two inherent dynamic states in lasers. We will first explain the experimental setup we used.

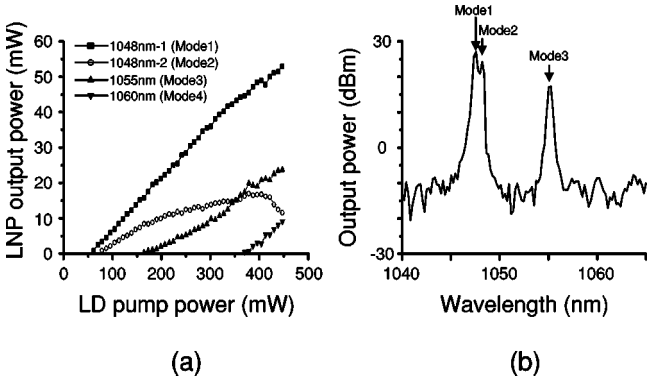

FIG. 2. (a) Input-output characteristics of an LNP laser. (b) Oscillation spectrum at pump power $P = 211$ mW.

A model laser system for investigating the multimode dynamics on a Λ transition was configured by controlling the operating condition of a LD-pumped 0.3-mm-thick LNP laser, with directly coated mirrors M_1 (reflectivity $R_1 > 99.9\%$ at lasing wavelengths, transmission $>95\%$ at 808 nm) and M_2 ($R_2 = 98\%$), subjected to frequency-shifted optical feedback as shown in Fig. 1. Two $PbMoO_4$ acousto-optic modulators (AOM1 is for upward frequency shift of $f_{AOM,1}$; AOM2 is for downward frequency shift of $f_{AOM,2}$) inserted in the optical feedback path introduced a round-trip frequency shift of $f_s = 2(f_{AOM,1} - f_{AOM,2})$ to the feedback light. In the present study on three-mode operations, we tuned f_s to $2f_{RO}$.

III. EXPERIMENTAL RESULTS FOR HARMONIC MODULATION

A. Input-output characteristics and oscillation spectrum

Global oscillation spectra were measured by a multiwavelength meter (HP-86120B: wavelength range 700–1650 nm) as a function of the pump power. Modal input-output characteristics and an example oscillation spectrum are shown in Figs. 2(a) and 2(b). Here, modes 1, 2, and 3 indicate the first oscillating mode on the ${}^4F_{3/2}(1) \rightarrow {}^4I_{11/2}(1)$ transition at 1048-nm wavelength, the second lasing adjacent mode on the same transition, and the third lasing mode on the ${}^4F_{3/2}(1) \rightarrow {}^4I_{11/2}(2)$ transition at 1055-nm wavelength, respectively. The dynamic instability due to quantum interference was not induced in the pump power level shown in Fig. 2(a).

B. Bifurcation diagram and dynamic states

Let us show an experimental bifurcation diagram and typical pulsation wave forms for different dynamic states when the LNP laser was subjected to harmonic modulations, in which the round-trip frequency shift f_s was tuned to twice the relaxation oscillation frequency—i.e., $f_s = 2f_{RO}$. An example bifurcation diagram is shown in Fig. 3 when the the light intensity impinged on the feedback mirror was changed by a variable optical attenuator, in which SRO, CSO, and CI denote the periodic sustained relaxation oscillation (soft mode), the chaotic spiking oscillation (hard mode), and the chaotic itinerancy between chaotic soft-mode and hard-mode oscillations. Because 5000 peak values collected from the long-term experimental time series were plotted in Fig. 3, the fluctuation of peak values in the SRO regime may have been caused by the pump fluctuation and the intrinsic noise. A subharmonic bifurcation structure leading to CI, which will be shown numerically in Sec. IV, was not identified experimentally.

In the transition process from the low-dimensional ordered states (i.e., periodic soft mode), exhibiting periodic sustained relaxation oscillations, to the high-dimensional global chaos (i.e., chaotic hard mode) featuring spiking oscillations, the system showed random switching between chaotic soft-mode and hard-mode oscillations. Here, each modal output was selected by a monochrometer and was measured by an InGaAs photodiode (New Focus 1811: DC-125 MHz) followed by a digital oscilloscope (Tektronix TDS

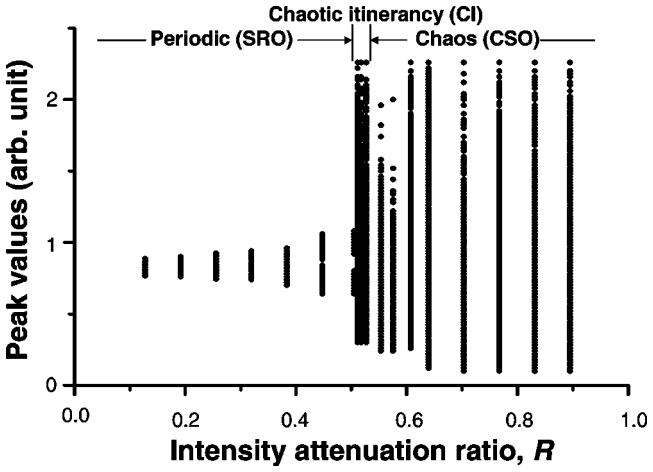

FIG. 3. Bifurcation diagram as a function of the light intensity attenuation ratio R by the variable attenuator. Here, successive peak values are plotted.

540D: DC-500 MHz). Typical oscillation wave forms in different dynamic states—i.e., SRO, CSO, and CI—are shown in Figs. 4–6 respectively. Note that three modes exhibit in-phase oscillations in the SRO regime as shown in the inset of Fig. 4. At the present pump power, the in-phase dynamics is maintained in the time domain of soft-mode chaos in CI, as shown in the inset of Fig. 6, suggesting phase synchronization [17] among three modes. The chaotic itinerancy took place generally for different pump-power levels as well, in which different types of collective chaos synchronization were often observed in the soft-mode chaos, depending on modal intensity ratios [14]. In the hard-mode (i.e., spiking) chaos (CSO) domain, on the other hand, no correlations were observed as shown in the inset of Fig. 5.

An example Poincaré section on the $[s_2, s_2']$ plane constructed from experimental time series in the chaotic itinerancy regime shown in Fig. 6 is depicted in Fig. 7, where s_2

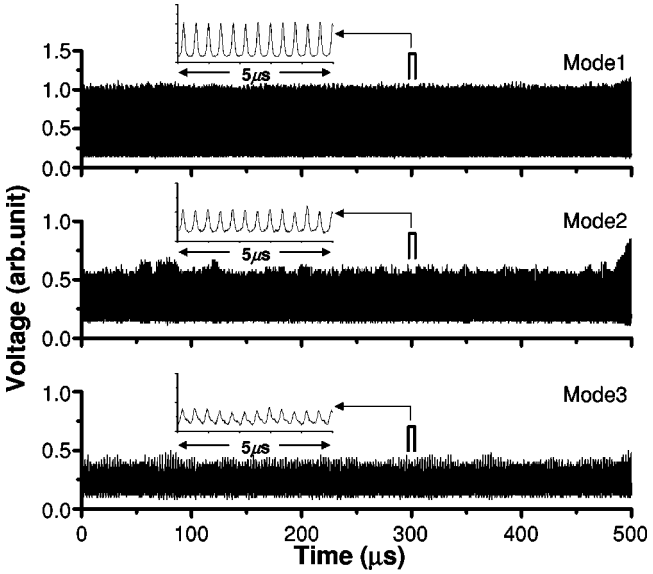

FIG. 4. Modal intensity wave forms in the sustained relaxation oscillation (SRO) regime. $P=161$ mW, $R=0.319$.

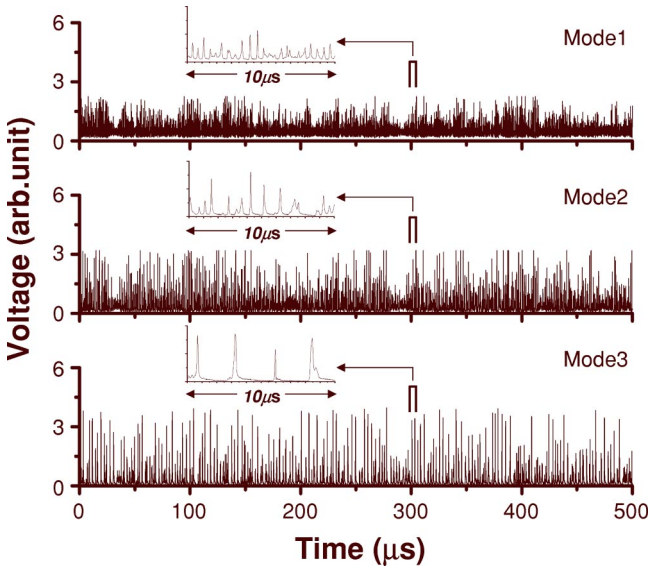

FIG. 5. Modal intensity wave forms in the chaotic spiking oscillation (CSO) regime. $P=161$ mW, $R=0.767$.

and s_2' are intensity of mode 2 and its time derivative. It should be noted that Poincaré sections of the soft-mode chaos [Figs. 7(a) and 7(c)] and the hard-mode chaos [Fig. 7(b)] show qualitatively different topologies. The structure which suggests intermittency or heteroclinic crossing was not identified. Therefore, the present switching behavior could be interpreted in terms of chaotic itinerancy [11].

C. Information circulation analysis

The observed bifurcation scenario leading to chaotic spiking oscillations via CI was already demonstrated in the single-mode regime [11]. Therefore, the present bifurcation route to global chaos is found to be generic in class-B lasers subjected to harmonic modulations, in which two ordered dynamic states—namely, soft- and hard-modes—coexist in

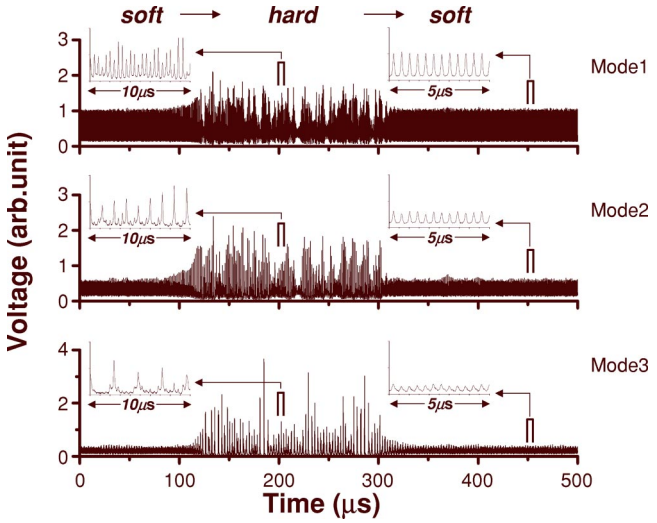

FIG. 6. Modal intensity wave forms in the chaotic itinerancy (CI) regime. $P=161$ mW, $R=0.527$.

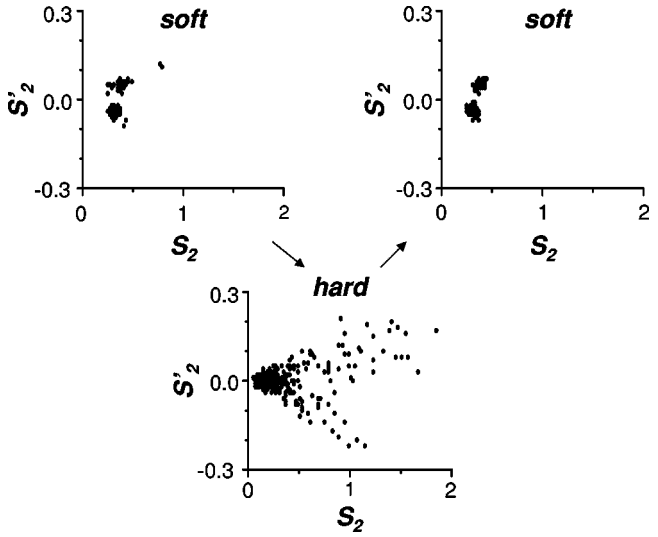

FIG. 7. Poincaré sections calculated from the experimental time series in the CI regime shown in Fig. 6.

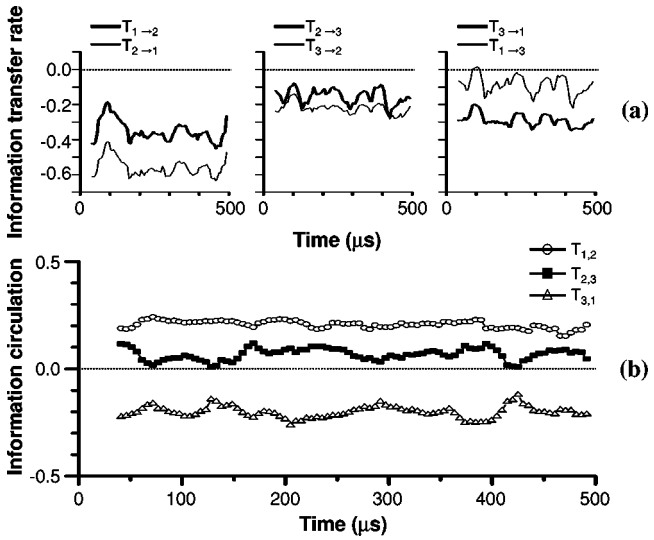

FIG. 8. Information flows among modes in the SRO regime calculated from the time series shown in Fig. 4. (a) Information transfer rates, (b) information circulations.

the phase space [11,16]. Then, the question arises, what kind of dynamic interplay does appear between oscillating modes in the chaotic itinerancy regime? In order to study this issue, we introduced the information-theoretic approach to characterize high-dimensional dynamic behaviors by using the coarse-grained information transfer rate among modes [13]—i.e., information circulation analysis [14].

The information circulation is defined as $T_{X,Y}=T_{X\to Y}-T_{Y\to X}$, $T_{X\to Y}=(1/\tau^*)\Sigma_\tau S(Y,Y_\tau|X)-(1/\tau^*)\Sigma_\tau S(Y,Y_\tau)$ is the coarse-grained information transfer rate from time series $X=\{x(t)\}$ to time series $Y=\{y(t)\}$, and $S(Y,Y_\tau)$ is the self-mutual information for Y. Here $S(Y,Y_\tau|X)$ is the conditional self-mutual information of time series Y given time series X [18] where τ^* is the first local minimum of $S(Y,Y_\tau)$ [19]. The information circulation $T_{i,j}$ is the "net" information flow among the two modes, and if $T_{i,j}>0(<0)$, the information flows from mode $i(j)$ to mode $j(i)$ [14].

Dynamic changes in information transfer rates and the resultant information circulations among modes calculated from experimental time series shown in Fig. 4 (SRO) are presented in Fig. 8. Note that the *strongest* intensity mode 1 acts as an information sender, which sends the information to other modes 2 and 3, while the *weakest* intensity mode 3 behaves as an information receiver which receives the information from other modes 1 and 2. The remaining *intermediate* intensity mode 2 receives the information from the sender mode 1 and transfers it to the receiver mode 3, acting as an information mediator. The present information network—i.e., causal information sender-mediator-receiver relationship—was found to be always established in the SRO regime. In the chaotic spiking oscillation (i.e., CSO) regime shown in Fig. 5, on the other hand, intermode information transfer rates among modes became greatly reduced as compared with those in the CRO regime and causal relationships among modes became unfixed, while the small amount of unidirectional information flow from mode 1 to mode 2 was maintained. Results are shown in Fig. 9.

In the chaotic itinerancy (CI) regime shown in Fig. 6, intermode information flows were found to change abruptly in accordance with switchings between chaotic soft- and hard-mode pulsations over times. Results are shown in Fig. 10. Despite random switchings, the information sender-mediator-receiver relationship shown in Fig. 8 was kept during nonperiodic soft-mode pulsations. However, this information network is destroyed and information flows similar to those in the CSO regime shown in Fig. 9 appear occasionally when spiking oscillations take place, in which the strongest mode 1 still acts as an information sender. This may imply that the strongest intensity mode plays the leading role acting as the information sender in the whole temporal evolution.

D. Joint time-frequency analysis

Let us examine the essential problem concerning the observed chaotic itinerancy in the multimode laser, in which all

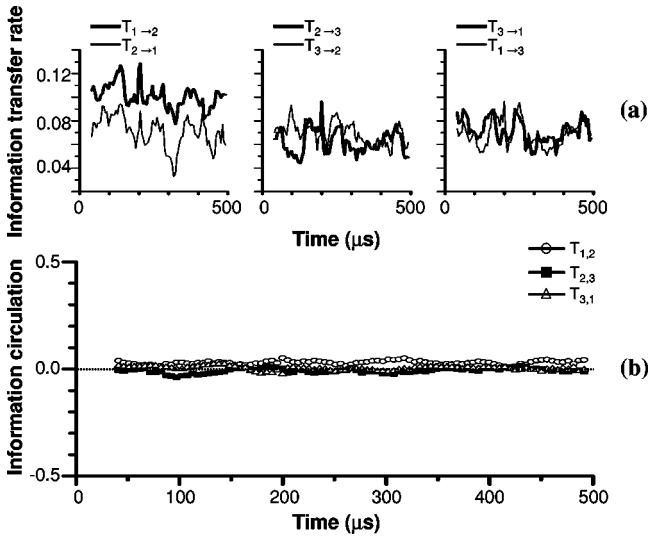

FIG. 9. Information flows among modes in the CSO regime calculated from the time series shown in Fig. 5. (a) Information transfer rates, (b) information circulations.

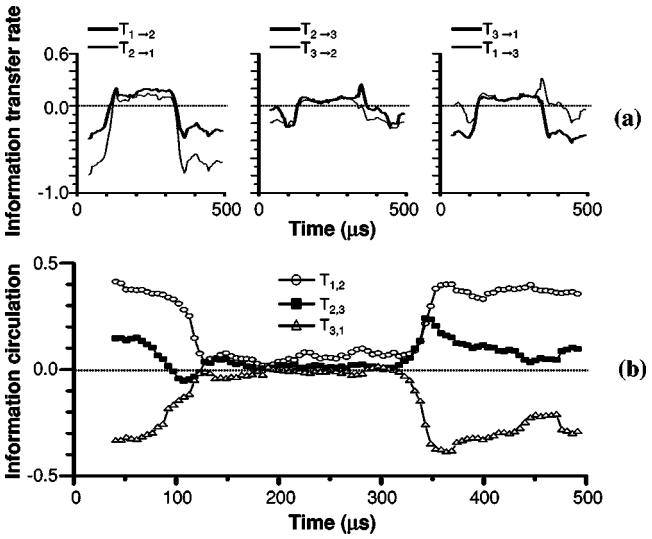

FIG. 10. Information flows among modes in the CI regime calculated from the time series shown in Fig. 6. (a) Information transfer rates, (b) information circulations.

the oscillating modes exhibit random switchings simultaneously over times as shown in Fig. 6, by using the joint time-frequency analysis (JTFA) of experimental time series [10]. The same characterization was done for the single-mode laser subjected to the harmonic modulation previously and we showed that frequency locking between the two periodicities of soft-mode relaxation oscillation and hard-mode spiking oscillation occurs in accordance with the switching [11].

In the present study, we applied JTFA to the three-mode case and the switching mechanism was identified paying the special attention to the modal JTFA signal. Typical results corresponding to the time series given in Fig. 6 are shown in Fig. 11, in which modal JTFA signals are presented. In the chaotic soft-mode regime, globally coupled modes exhibited the periodicity of f_{RO} and its higher harmonics, featuring the phase synchronization mentioned in Sec. III, which satisfies the inherent antiphase dynamics. In the chaotic hard-mode regime, a power spectrum broadened featuring the lower fundamental pulsation frequency $f_{SO}<f_{RO}$, in which the phase synchronization failed. It is obvious from Fig. 11 that the

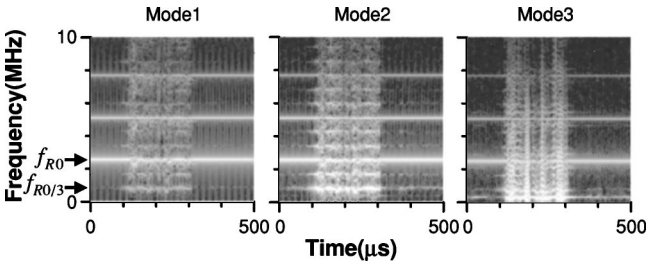

FIG. 11. Joint time-frequency analysis of the time series shown in Fig. 6 in the CI regime. Calculations were carried out using a moving window with a length of $T_w=2048$ data points (40.96 μs) and a moving step T_s with a length of 256 data points (5.12 μs), where the light intensity was partitioned into $I_s=16$ values to calculate intensity probability distributions.

switching from soft-mode to hard-mode pulsation takes place when the subharmonic component of chaotic soft-mode oscillation was enhanced during the course of temporal evolution and excited spiking the hard mode through frequency locking of $f_{RO}/3=f_{SO}$. In short, switching takes place through temporal frequency locking of the two periodicities similar to the single-mode case [11]. The key feature in the multimode case is that switching occurs when the highest relaxation oscillation frequency f_{RO} indicates subharmonic locking with the spiking frequency f_{SO}, while lower relaxation oscillation components f_2 and f_3 do not play the essential role in switchings. Therefore, the inherent antiphase dynamics holds in the chaotic itinerancy regime such that the total output behaves just like a single-mode laser [16] and all the modes exhibit cooperative switchings simultaneously.

IV. NUMERICAL SIMULATION

A. Rate equation for lasers subjected to harmonic modulation

The fundamental equation for the model of class-B lasers subjected to frequency-shifted optical feedback is given by coupled stochastic delay-differential equations for population inversion, electric field including phase and spontaneous emission noise as described in Ref. [11]. Under the weak feedback condition—i.e., frequency shift $f_s \gg m/\tau_p$ ($m=E_s/E_o$, field amplitude feedback ratio τ_p, photon lifetime)—the equations become equivalent to those of loss-modulated lasers at frequency f_s. Then, the following simplified rate equations are derived in the short-delay limit—i.e., $t_D \ll f_{RO}^{-1}$ [15]—such as in the present experiment:

$$\frac{dn_k}{dt} = w - n_k - g_k n_k\left(s_k + \sum \beta_{k,j} s_j\right), \tag{1}$$

$$\frac{ds_k}{dt} = K\{[g_k n_k - \Gamma_k]s_k + \eta s_k \cos \Omega_s t\}, \tag{2}$$

$$k = 1,2,3, \quad j \neq k.$$

Here, w is the relative pump power normalized by the first-mode threshold, n_k is the normalized population inversion density of the kth mode, s_k is the normalized photon density, K is the fluorescence-to-photon lifetime ratio, τ/τ_p, time is scaled by the fluorescence lifetime, g_k is the modal gain ratio with respect to the first mode, Γ_k ($=[L_0+2\alpha_k L]/[L_0+2\alpha_1 L]$) is the modal loss ratio (L_0, common cavity loss; α_k, reabsorption coefficient; L, crystal length), $\beta_{k,j}$ is the cross-saturation coefficient, $\eta=m^2$ is the intensity feedback ratio, and $\Omega_s=2\pi f_s \tau$ is the normalized frequency shift. The spontaneous emission noise is neglected. Additionally, the nonlinear stimulated absorption coefficient resulting from quantum interference among lower-level atoms [15] is omitted without essential loss of the physics of loss-modulated lasers because we examine dynamics below the Hopf bifurcation point.

B. Bifurcation diagram and dynamic states

Calculated input-output characteristics for modal intensities s_1, s_2, and s_3 are shown in Fig. 12, where relevant spec-

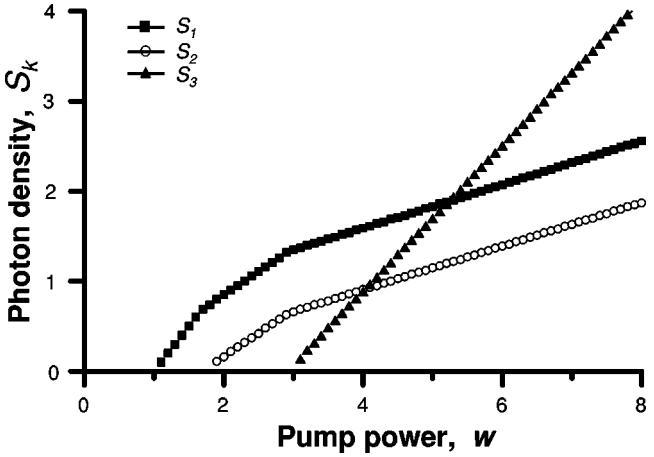

FIG. 12. Numerically calculated input-output characteristics. Adopted parameter values are $K=1000$, $g_1=1$, $g_2=0.95$, $g_3=0.50$, $\beta_{1,2}=0.923$, $\beta_{1,3}=\beta_{2,3}=2/3$, $L=0.03$ cm, $L_0=0.0297$, $\alpha_1=\alpha_2=0.11$ cm^{-1}, and $\alpha_3=0.0407$ cm^{-1}.

troscopic data for LNP lasers are assumed. Here, modes 1 and 2 are on the 1048-nm transition and mode 3 is on the 1055-nm transition similar to the experimental situation. A bifurcation diagram as a function of the intensity feedback ratio is shown in Fig. 13 together with the largest Lyapunov exponent, where the period-1-cycle SRO region in the regime of low feedback ratio is omitted. The observed bifurcation diagram from SRO to CSO via chaotic itinerancy is well reproduced by numerical simulation shown in Fig. 13. Example wave forms in the CI regime are indicated in Fig. 14(a).

In order to extract further information inherent in chaotic itinerancy from numerical time series, we calculated temporal evolutions of largest "local" Lyapunov exponents for different dynamic states. Here, the *i*th one-dimensional local Lyapunov exponent is defined in terms of the length of the

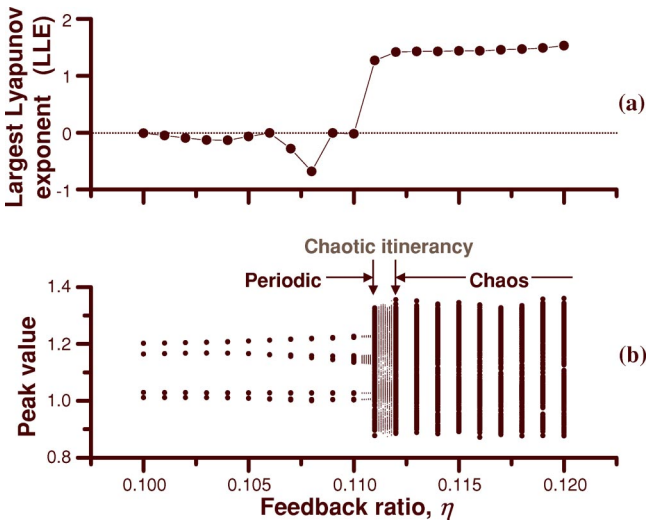

FIG. 13. The largest Lyapunov exponent (a) and bifurcation diagram (b) as a function of the feedback ratio, η, calculated from numerical time series. $w=3.12$. Other adopted parameter values are the same as Fig. 12.

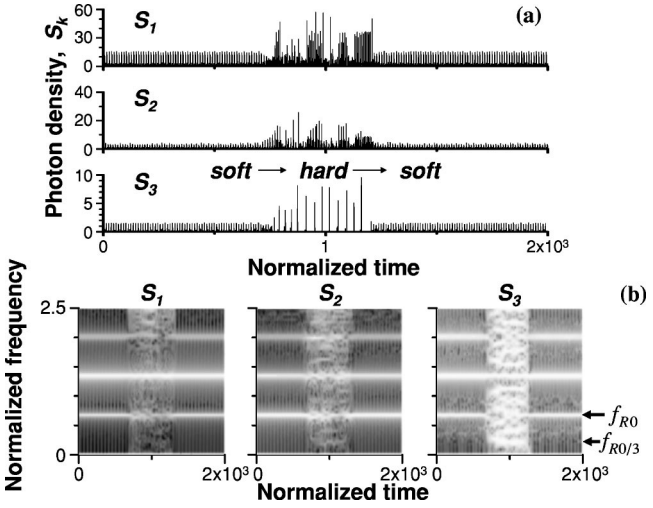

FIG. 14. (a) Numerical result of modal intensity wave forms in the CI regime. (b) Joint time-frequency analysis of the numerical time series shown in (a). $w=3.12$, $\eta=0.111$.

ellipsoidal principle axis of an *n*-ellipsoid ($n=6$ in the present case) $P_i(t)$:

$$\lambda_i(t) = \frac{1}{\Delta t}\log_2\frac{P_i(t+\Delta t)}{P_i(t)}. \tag{3}$$

Results are shown in Figs. 15(a)–15(c), together with standard deviations as a function of feedback ratio [Fig. 15(d)]. Here, the averaging time Δt for calculating local Lyapunov exponents was 80. It is obvious that the local Lyapunov exponent in CI fluctuates wildly in time as compared with other states, reflecting the nonstationary nature of chaotic itinerancy.

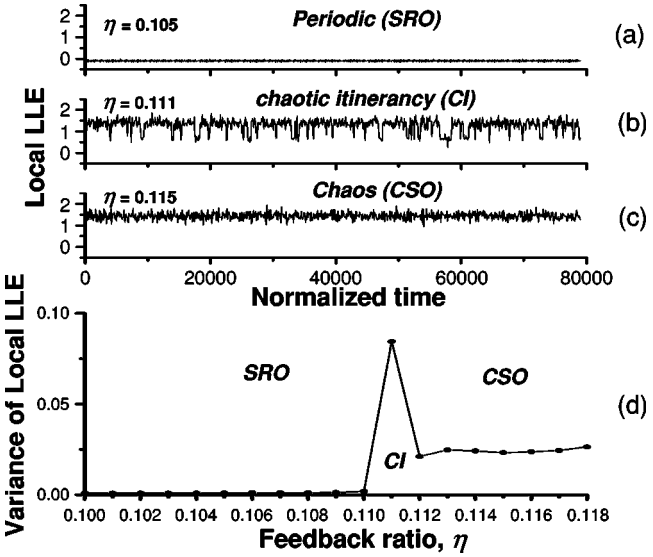

FIG. 15. (a), (b), (c) Temporal evolutions of local Lyapunov exponents in three regimes. (d) Standard deviation as a function of the feedback ratio. $w=3.12$.

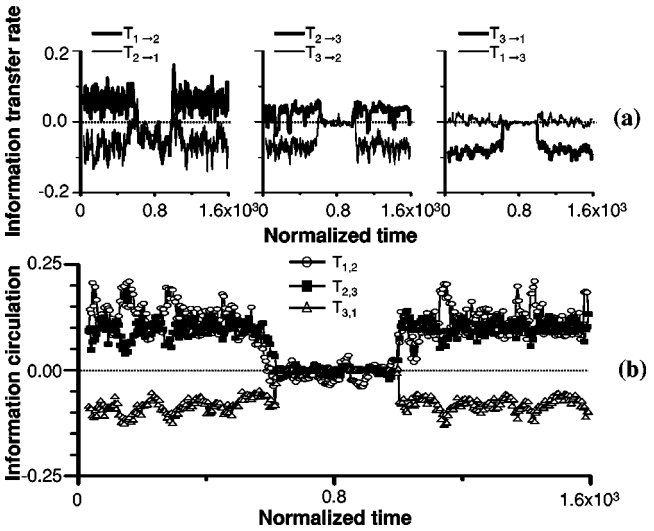

FIG. 16. Numerical result of information flows among modes in the CI regime. $w=3.12$, $\eta=0.111$. $T_w=2048$ data points and a moving step T_s with a length of 256 data points, where the light intensity was partitioned into $I_s=16$ values to calculate intensity probability distributions.

C. Information circulation and joint time-frequency analysis

Finally, let us show information flows among modes indicating the establishment of a causal information sender-mediator-receiver relationship and parametric resonance of two periodicities of SRO and CSO by using numerical time series in the CI regime.

Figure 16 shows coarse-grained information transfer rates and the resultant information circulations among modes calculated from numerical time series shown in Fig. 14(a). Experimental results shown in Fig. 10 are found to be reproduced by the simulation qualitatively. The simulated JTFA signals are shown in Fig. 14(b) which indicates temporal 1/3 frequency locking among two periodicities between chaotic soft-mode and hard-mode pulsations associated with switchings.

The present numerical simulation without noise can reproduce the essential features of the observed "deterministic" chaotic itinerancy qualitatively in a wide parameter region. In order to achieve further detailed quantitative agreement with the experimental time series, however, a further precise tuning of operating parameters—e.g., w, L_0, and η—is needed. Additionally, in a real experimental system, the spontaneous emission noise has an additional effect on the chaotic itinerancy because the periodicity of the spiking oscillation depends on the spontaneous emission rate [11]

V. CONCLUSION

In conclusion, we investigated the chaotic itinerancy route to chaotic spiking oscillations in a three-mode laser subjected to frequency-shifted optical feedback. Dynamic characterizations of bifurcated dynamic states were carried out by using experimental time series of modal outputs. The information-theoretic analysis in terms of coarse-grained information transfer rates and the resultant information circulation has identified the causal information sender-mediator-receiver relationship among modes established depending on the difference in modal intensities. The joint time-frequency analysis revealed that the occasional frequency locking of two periodicities of relaxation oscillations and spiking oscillations for the total output over times provides the key mechanism with simultaneous random switchings among the two chaotic states. The essential features of observed phenomena were reproduced qualitatively by simulation of the simplified model equations of multimode lasers subjected to harmonic-frequency loss modulation.

Generic features of intermittency or heteroclinic crossing were not identified in Poincaré sections which were constructed by using experimental time series. The nonlinear physical mechanism—i.e., "temporal locking of two periodicities" in the present laser system—might play an essential role in creating an easy switching path among two dynamic states in the present chaotic itinerancy similar to other laser models [2,3,9]. In the usual intermittent or heteroclinic chaos, the switching path is well defined in the phase space according to the bifurcation rule of dynamic equations. The change in switching probability against the change in feed-

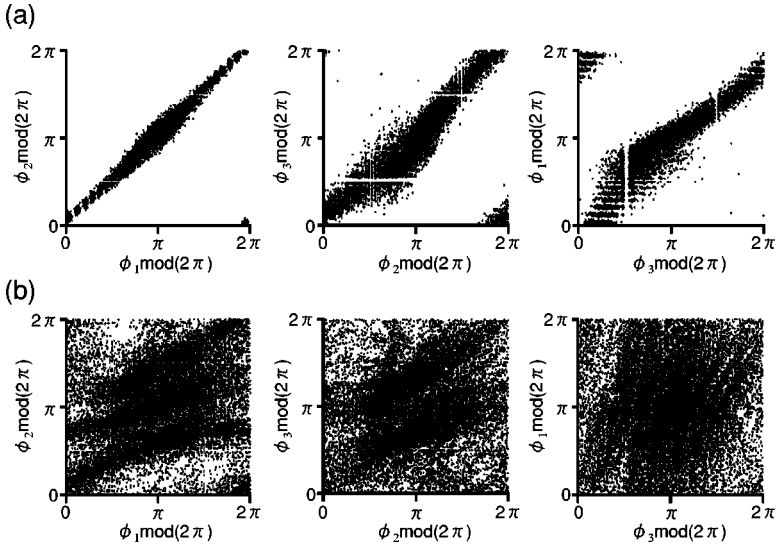

FIG. 17. Phase correlation plots indicating chaotic itinerancy between phase-synchronized and -unsynchronized chaos calculated from the time series shown in Fig. 6. (a) Soft-mode chaos domain, (b) hard-mode chaos domain.

back ratio from the critical value for the occurrence of CI, calculated from extremely long-term time series, would provide insight into general features of the chaotic itinerancy.

APPENDIX: DYNAMIC SWITCHING BETWEEN PHASE SYNCHRONIZED AND UNSYNCHRONIZED CHAOS

In the chaotic itinerancy observed under the pumping condition shown in Fig. 6, strong phase correlations appeared among modal output wave forms in the time domain of soft-mode chaos. In this appendix, we show phase correlation plots indicating such an interesting switching behavior between phase-correlated chaos and unsynchronized chaos over time.

Let us examine the phase correlation among modal intensity wave forms by extracting the analytical phase from experimental time series. Using the Hilbert transformation of time series—i.e., Gabor's analytic signal used in the analysis of phase synchronization [17]—we calculated the analytic phase correlation of three modes. The analytic phase $\phi(t)$ is related to the analytic signal V_A and its time average $\langle V_A \rangle$ by $V_A(t) - \langle V_A \rangle = R_A(t) e^{i\phi(t)}$. Here, $V_A(t) = I(t) + iI_H(t)$ where $I(t)$ is the time series of scalar intensity and I_H is the its Hilbert transform. Results obtained from the time series shown in Fig. 6 are shown in Figs. 17(a) and 17(b) for soft- and hard-mode chaos, respectively, where (a) indicates the phase correlations of long-term modal output time series before switching to the hard-mode chaos in Fig. 6. The same correlations were obtained for time series of soft-mode chaos after the hard-mode chaos in Fig. 6. There were no intensity correlations among modes for both cases, so intensity correlation plots are not shown. It is apparent that the soft-mode chaos centers the plot about the diagonal, especially for modes 1 and 2, demonstrating phase synchronization in the time domain of chaotic SRO, as shown in Fig. 17(a). In the domain of CSO (i.e., hard-mode chaos), synchronization fails as shown in Fig. 17(b).

[1] For the most recent review, see K. Kaneko and I. Tsuda, *Chaotic Itinerancy* [Chaos **13**, 926 (2003)] and references therein.

[2] K. Ikeda, K. Otsuka, and K. Matsumoto, Prog. Theor. Phys. Suppl. **99**, 295 (1989).

[3] K. Otsuka, Phys. Rev. Lett. **65**, 329 (1990).

[4] K. Kaneko, Physica D **41**, 137 (1990).

[5] K. Kaneko, Physica D **54**, 5 (1991).

[6] I. Tsuda, World Futures **32**, 167 (1991).

[7] F. T. Arecchi *et al.*, Phys. Rev. Lett. **65**, 2531 (1990).

[8] F. T. Arecchi, Physica D **51**, 450 (1991).

[9] I. Fisher *et al.*, Phys. Rev. Lett. **76**, 220 (1996).

[10] K. Otsuka, T. Ohtomo, T. Maniwa, H. Kawasaki, and J.-Y. Ko, Chaos **13**, 1014 (2003).

[11] K. Otsuka, J.-Y. Ko, and T. Kubota, Opt. Lett. **26**, 638 (2001); J.-Y. Ko, K. Otsuka, and T. Kubota, Phys. Rev. Lett. **86**, 4025 (2001).

[12] K. Ikeda and K. Matsumoto, Phys. Rev. Lett. **62**, 2265 (1989).

[13] M. Palus, V. Komarek, Z. Hrncir, and K. Sterbova, Phys. Rev. E **63**, 046211 (2001).

[14] K. Otsuka, T. Ohtomo, A. Yoshioka, and J.-Y. Ko, Chaos **12**, 678 (2002).

[15] K. Otsuka, Y. Miyasaka, T. Kubota, and J.-Y. Ko, Phys. Rev. E **69**, 046201 (2004).

[16] K. Otsuka, *Nonlinear Dynamics in Optical Complex Systems* (Kluwer Academic, Dordrecht, 1999).

[17] M. G. Rosenblum, A. S. Pikovsky, and J. Kurths, Phys. Rev. Lett. **76**, 1804 (1996).

[18] In the previous papers [10,14], the definition of $S(Y, Y_\tau | X)$ included the same typographical error. The correct definition of $S(Y, Y_\tau | X)$ should be the conditional self-mutual information of time series Y given time series X.

[19] A. M. Fraser and H. L. Swinney, Phys. Rev. A **33**, 1134 (1986).